Capturing Structural Heterogeneity in Chromatin Fibers

Ekundayo, Babatunde; Richmond, Timothy J.; Schalch, Thomas

How to cite

EKUNDAYO, Babatunde, RICHMOND, Timothy J., SCHALCH, Thomas. Capturing Structural Heterogeneity in Chromatin Fibers. In: Journal of Molecular Biology, 2017, vol. 429, n° 20, p. 3031–3042. doi: 10.1016/j.jmb.2017.09.002

This publication URL: https://archive-ouverte.unige.ch/unige:97268
Publication DOI: 10.1016/j.jmb.2017.09.002

Accepted Manuscript Version for Ekundayo, B., Richmond, T.J., and Schalch, T. (2017). Capturing Structural Heterogeneity in Chromatin Fibers. Journal of Molecular Biology.

http://dx.doi.org/10.1016%2Fj.jmb.2017.09.002

Capturing Structural Heterogeneity in Chromatin Fibers

Babatunde Ekundayo[1,2], Timothy J. Richmond[3], Thomas Schalch[1,2%]

[1] Department of Molecular Biology, Faculty of Sciences, University of Geneva, CH-1211 Geneva 4, Switzerland

[2] Institute of Genetics and Genomics of Geneva (iGE3), University of Geneva, CH-1211 Geneva 4, Switzerland

[3] Institute of Molecular Biology and Biophysics, Department of Biology, Swiss Federal Institute of Technology Zurich, CH-8093 Zurich, Switzerland

[%] Corresponding author:

Email: thomas.schalch@unige.ch, Tel: +41 22 379 6127

Short Title:

Structural heterogeneity in chromatin fibers

Keywords:

Tetranucleosomes; Chromatin structure; Nucleosomes

Summary

Chromatin fiber organization is implicated in processes such as transcription, DNA repair and chromosome segregation, but how nucleosomes interact to form higher order structure remains poorly understood. We solved two crystal structures of tetranucleosomes with approximately 11 base pair DNA linker length at 5.8 and 6.7 Å resolution. Minimal intramolecular nucleosome-nucleosome interactions result in a fiber model resembling a flat ribbon that is compatible with a two-start helical architecture, and that exposes histone and DNA surfaces to the environment. The differences in the two structures combined with electron microscopy reveal heterogeneous structural states, and we used site-specific chemical crosslinking to assess the diversity of nucleosome-nucleosome interactions through identification of structure-sensitive crosslink sites that provide a means to characterize fibers in solution. The chromatin fiber architectures observed here provide a basis for understanding heterogeneous chromatin higher order structures as they occur in a genomic context.

Introduction

The eukaryotic genome is packaged into chromatin higher order structures that are composed of nucleosomes connected by varying lengths of linker DNA [1–3]. Histones H3 and H4, as well as H2A and H2B form heterodimers that in turn assemble into the histone octamer, around which 145-147 bp of DNA is wrapped in ~1.67 left handed helical turns to form the nucleosome core particle [4]. Nucleosome-nucleosome interactions are important for chromatin folding as exemplified by the thoroughly studied interaction between the H4 tail and the H2A-H2B acidic patch which was first observed in a crystal contact between nucleosome core particles [4,5]. This interaction is essential for the formation of higher order structures and is regulated by acetylation of H4 lysine 16 [6–8]. The acidic patch is also a binding hub on the nucleosome for chromatin associated proteins [9,10]. The tetranucleosome structure has revealed a nucleosome-nucleosome contact mediated by the histone H2B α C helix [11], and an identical interaction has been observed in cryo-EM structures of chromatin fibers that make use of both the H2B α C and H4-acidic patch mediated contacts [12]. Ubiquitylation of H2B disrupts the H2B α C contact and leads to loosening of chromatin structure [13].

Tetranucleosomes are postulated to be functional and structural units of the genome that can regulate gene expression [12,14,15], and recent data suggests that most genomes organize nucleosomes in small clusters and are devoid of long-range nucleosome-nucleosome organization [16–19]. There is a large variability in chromatin fiber structure since it strongly depends on the DNA linker length and sequence between nucleosomes and on environmental conditions given by the ionic and cellular environment. Nevertheless, nucleosomes in live cells form detectable higher-order structures [20,21].

To date, detailed experimental structural information is available for a tetranucleosome with 167 base pair repeat length [11] and for 12-mer 177 and 187 base pair NRL arrays [12]. These structures share a highly similar fiber architecture, which is likely a result of them being related to each other by integral multiples of the 10 bp helical twist of DNA. Every base pair change in the length of the linker DNA is predicted to induce a 34 degree change in the relative angle between the flanking nucleosomes (Fig. S1a), and therefore non-integral multiples of 10 bp DNA linker lengths are predicted to produce significantly different fiber structures [22–24], but detailed structural evidence is lacking. Since chromatin structure is involved in the regulation of fundamental genomic processes [25], the structural changes in chromatin imposed by varying linker lengths is predicted to play an important role as it might directly influence how for example the gene regulatory or replication machinery interacts with the chromatin template [26,27].

The influence of nucleosome repeat length on modulating nucleosome-nucleosome interactions and thus the accessibility of the underlying DNA remains poorly understood. Chromatin with short linker lengths less than ten base pairs are found in the nuclei of various organisms such as *Schizosaccharomyces pombe* [28–30] and *Aspergillus nidulans* [31,32], in specific mammalian cell types such as in the neuronal cortex [33], and in genomic regions such as at telomeres [34]. Although these short repeat lengths occur under many circumstances in nature, their consequence on chromatin fiber structure is poorly understood.

In order to understand chromatin fiber architectures with short nucleosome repeat lengths in more detail, we crystallized corresponding tetranucleosomes and solved their structures. The resulting structures reveal highly accessible DNA and histone surfaces, and the crystal packing suggests new modes of nucleosome face-to-face interactions that predominantly involve the H2B helices. We show by site-specific cross-linking that histone-histone contacts vary significantly

with nucleosome repeat length and chromatin fiber state, thereby revealing how the accessibility of the histone octamer surface is modulated.

Results

Short NRL tetranucleosomes crystallize in various forms

Due to the helical nature of DNA the relative rotation between consecutive nucleosomes in the chromatin fiber is strongly dependent on the linker DNA length and is predicted to fundamentally constrain how nucleosomes can interact to form higher order structures [22]. In order to visualize chromatin fiber structure and nucleosome-nucleosome interactions as a function of DNA linker length we crystallized tetranucleosomes of varying DNA linker lengths. As DNA flexibility will be reduced with short linker lengths, we decided to reconstitute and crystallize a panel of tetranucleosomes covering NRLs from 147 to 158 base pairs (Fig. S1b-d). These NRLs are likely to correspond to DNA linker lengths of 2-13 nucleotides, as the 601 nucleosome positioning sequence used for our crystallization studies wraps 145 base pairs of DNA in the nucleosome core [35,36].

Many of the short repeat-length tetranucleosomes formed crystals readily under conditions previously identified to be conducive to tetranucleosome crystallization [11]. The various crystals show different morphologies ranging from rectangular or hexagonal blocks to fine needles (Fig. 1a). Diffraction analysis of the crystals confirmed that the morphological differences corresponded to differences in crystal packing, which manifests themselves in strong variation in diffraction power and space group parameters. For tetranucleosomes with NRLs of 150, 153, 155, 156, 157 and 158 base pairs we observed diffraction while tetranucleosome with 147, 151, 152 and 154 base pair NRL did not diffract measurably (Fig. 1b). Amongst the diffracting

crystals we were able to determine space group parameters for 155-, 156- and 157- NRL crystals. The 155 and 156 NRL crystals belong to the hexagonal system and have almost identical, large unit cell dimensions, except for the c axis, which is double the value in the 155-NRL crystals compared to the 156-NRL crystals.

The 157NRL tetranucleosome yielded two different crystal forms, one with space group P1 containing four nucleosomes in the asymmetric unit (AU) and the second with space group C2 containing two nucleosomes per AU. The P1 form diffracted to 5.8 Å and the C2 form to 6.7 Å resolution. We were able to solve both crystal structures by molecular replacement using the 601 nucleosome core particle [35,37] as a search model (see Table 1 for data collection and refinement statistics) (Fig. 2a,b). Clear DNA density was visible after molecular replacement and rigid body refinement of nucleosome positions (Fig. S2a). Since the tetranucleosomal DNA used in these experiments is not symmetric, the C2 structure represents a pseudosymmetry with superposition of the two asymmetric sequence halves by the crystallographic two-fold (Fig. 2b).

157-NRL tetranucleosomes show open architecture with exposed nucleosome surfaces

The two 157-NRL tetranucleosome structures reveal similar arrangements of nucleosomes (Fig. 2a,b) with two pairs of nucleosomes that have their dyads facing towards each other, and the linker DNA running across the space between the nucleosomes (Fig. 2c). This overall configuration is similar to the 167-NRL tetranucleosome [11] (Fig. 2d). The DNA densities follow an overall straight path from one nucleosome exit to the next nucleosome entry. However, the exit/entry points show significant bending in order to accommodate the otherwise straight trajectory. We observe different degrees of bending for the various linkers, with the P1 structure showing stronger exit/entry bends than the C2 structure, in particular in the middle linker

segment. The linker DNA density is best modeled by B-form DNA of 11 bp in length in both crystal forms and for all linkers that we observe. The resolutions of 5.8 and 6.7 Å for these structures do not permit us to see individual rungs of the DNA ladder, and we therefore estimate the linker to contain 10-12 nucleotides with the most likely value being 11 nucleotides. This suggests that one of the flanking nucleosomes might compress its DNA to accommodate 146 base pairs of DNA in the core instead of the 145 observed in the 601 crystal structure. The paths of the various linker densities suggest that the nucleosome entry/exit points are the points where distortion of DNA most easily occurs.

For both 157-NRL tetranucleosome structures the histone octamer and the DNA surface of the nucleosome cores are accessible and are not occluded by core-core packing (Fig. 2 a,b). Contacts between cores are limited to neighboring nucleosomes in the +/-2 position, and these contacts localize to a DNA-DNA interface around superhelix location +2 or -2 on the two interacting nucleosomes. This area is adjacent to where the H4 N-terminal tail exits from the histone octamer core, and the H4 tail might be mediating this interaction. However, we cannot directly observe the H4 tail at the given resolution of the crystal structures.

In order to further validate the 157-NRL tetranucleosome structures we imaged 157-NRL tetranucleosomes by negative stain electron microscopy (Fig. 2e). We observed particles that resemble the overall shape expected from crystallography, and the class averages show four densities in similar open arrangement to that observed in the crystal. Therefore, crystal packing forces are unlikely to be a dominant determinant of the open tetranucleosome structure.

In summary, we have determined two tetranucleosome structures for the 4n157 NRL with largely exposed nucleosome core surfaces.

157NRL chromatin fibers are more compact than 157NRL tetranucleosomes

In order to understand the significance of our tetranucleosome structures for chromatin fiber folding, we used the crystal structures to determine parameters for a regular chromatin fiber model. In a first step we defined the fiber axis by the mid-points between nucleosome core centers of consecutive nucleosomes that face each other across the gap bridged by the DNA linkers (Fig. S3a-d). This helix axis definition is compatible with DNA ends being able to join and to form a long, continuous strand of DNA. The fiber axis serves as reference for calculation of nucleosome positions and orientations. We find that in the C2 crystal form, the nucleosome spacing along the fiber axis corresponds to 33 Å between N1 and N2, while the distance between N2 and N2' is 63 Å (Fig. S3b,d). These numbers reveal a variable helical rise and indicate that in the C2 structure the tetranucleosomes have transitioned into a less regular configuration by increasing the rise between the central pair of nucleosomes. This arrangement permits a straighter linker path than would a uniform repeat and creates a two-fold pseudo-symmetric particle. In the P1 structure, the distances are more regular with 40, 49 and 39 Å steps between nucleosomes along the fiber axis. The two structures are also distinguished by the different β angles of the nucleosomes. In the P1 structure, they vary between 56° and 64°, while they have values of between 67° and 72° in the C2 structure. A smaller β angle corresponds to a larger inclination of the nucleosomal DNA superhelix with respect to the fiber axis and allows for tighter packing in the P1 structure.

Both structures are consistent with a fundamental two-start fiber arrangement that has been observed for chromatin fiber structures using longer DNA linkers [6,11,12]. In contrast to the former structures, the 157-NRL tetranucleosome shows minimal intra-molecular nucleosome interactions. The P1 form proves to be significantly more compact due to larger core-core

interface and stronger bending in the linker DNA when compared to the C2 form, showing that tetranucleosomes can assume different structures. Building a model in the FiberModel package [38] using average parameters obtained from the 157-NRL tetranucleosomes results in a flat ribbon with an overall diameter of 23 Å. The β Euler angles for nucleosomes can only be accommodated in the fiber if we allow for a shallow left-handed twist (Fig. 3a).

Analytical ultracentrifugation experiments show that both 157NRL tetranucleosomes and 157NRL 12-mer arrays compact in solution (Fig. S3e,f). These S values correspond to the S values expected for these kind of structures as determined by calculating theoretical S values with HYDRO++ for bead models of corresponding chromatin fibers (data not shown) [39].

In order to compare the structure of the tetranucleosome with the arrangement of nucleosomes within longer fibers we analyzed 157NRL 12-mer arrays by electron microscopy. Negative stain imaging followed by 2D classification show that many particles formed by these arrays consist of two elongated densities that converge at a common point (Fig. 3b,c). One or both of the elongated densities show a striped pattern for a significant number of particles. In many cases, 5-6 densities that fit nucleosome dimensions can be counted in the elongated densities reminiscent of the two-start ladders observed previously [6]. The predominant class average (Fig. 3c) shows two strands, one of them with 5 globular densities spaced at distances of about 65 Å. This value is somewhat lower than expected from the crystal structures where we see corresponding distances of ~87 Å in the P1 form or ~96 Å in the C2 form. At the resolution of our negatively stained 12-mer arrays we see that nucleosome packing is in agreement with an overall two-start architecture, but we cannot determine how nucleosomes pack in detail. The interactions between nucleosomes are likely to have taken on a more compact state with the twisting stronger than predicted from the modeling. These differences may be due to the glutaraldehyde crosslinking or

due to a different mode of nucleosome-nucleosome interactions in longer fibers compared to the tetranucleosomes.

Tetranucleosome crystals rely on extensive nucleosome face-to-face packing

Analysis of the 157NRL tetranucleosomes in the crystals reveals that nucleosomes of neighboring asymmetric units stack on top of each other using extensive histone octamer interactions or DNA-DNA contacts (Fig. 4). For both the P1 and the C2 crystal forms these interfaces involve predominantly the H2A/H2B dimers which form a continuous column throughout the crystal lattice (Fig. 4a,b,d,e). However, the details of these interactions differ between the P1 and the C2 crystals. The nucleosomes in the P1 form are stacked at a steeper angle, yielding less overlap between nucleosomes than for the C2 form. In the P1 form, the H2Bα 1 helices of opposite nucleosome faces are juxtaposed and H2B α C helices stack onto the DNA of neighboring nucleosomes. In the C2 form, H2A/H2B interfaces are shifted with respect to each other such that H2B α 1 is opposite of H2B α C, and opposing H2B α C C-termini approach each other closely.

In order to quantitatively analyze and compare the distances separating identical H2B residues in our and other published structures, we have determined distances between identical residues of H2B across the nucleosome-nucleosome interface (Fig. 5a). The heatmap reveals that each of the tetranucleosome structures has a unique distance signature. The P1 crystal packing is characterized by close contacts around Q44 in the α 1 helix of H2B, while the C2 contacts mostly involve the α C helix of H2B with closest contacts around A121 at the C-terminus. The C2 contacts resemble the contact interface observed in the 167-NRL tetranucleosome, but they distinguish themselves by the closer contact at H2BA121 due to the alignment of the dyad axes

between stacked nucleosomes in the 157-NRL C2 structure. These signatures suggest that cross-linking of identical residues in H2B might be used as a sensitive tool to detect specific nucleosome packing modes under diverse experimental conditions (Fig. 5b).

Nucleosome-nucleosome crosslinks are sensitive to environment and repeat length

At the resolution of our structures we cannot determine interactions at single residue level with confidence. In order to verify the existence of specific nucleosome-nucleosome contacts for chromatin fibers in solution we used disulfide cross-linking chemistry and reconstituted a panel of cysteine mutations with five different NRLs between 157 and 177 bp. As sites of crosslinking we chose residues Q44, K113 and A121 on H2B as well as the previously established histone H4V21C and H2AE64C mutants [6] (Fig. 5c). The H2B sites were chosen with the goal to distinguish the different packing modes observed in the known tetranucleosome structures (Fig. 5a) with H2B Q44 being diagnostic of the 157NRL/P1 structure, while H2B K113 and A121 are predicted to be diagnostic of intermolecular contacts as observed in the 167-NRL tetranucleosome. The 157-NRL tetranucleosome structures suggests that the H4 tails of nucleosomes in +/-2 positions in the fiber are in crosslinking distance. We therefore also tested H4V21C alone as a site characteristic of intramolecular contacts in both 157-NRL structures.

Chromatin fibers undergo reversible structural transitions depending on ionic concentrations in the medium. In the absence of salt chromatin fibers assume an extended beads-on-a-string conformation. At low concentrations of divalent ions the nucleosomal arrays compact into 30-nm fibers, while elevated divalent ion concentrations induce reversible self-assembly of fibers into large oligomeric clusters [8,40,41]. In order to monitor nucleosome-nucleosome contacts in these

different structural states we used magnesium-free conditions to monitor the open state, 1 mM magnesium chloride to induce a compact state and 8 mM magnesium to trigger oligomerization.

For each cysteine mutant octamer we determined the crosslinking profile for diverse repeat lengths and for open, compacted and oligomerized states (Fig. 5d, S5). The H2AE64C-H4V21C disulfide crosslink could be observed for all NRLs tested between 157 and 177 NRL, and it is particularly pronounced in the oligomerized states. Albeit weaker the H4V21C single mutant crosslinks in a similar fashion, except that disulfide bridges do not form in the open state where we observe significant crosslinking in the H2AE64C-H4V21C background. In the compacted states of 157-, 167- and 177-NRL arrays, the H4V21C crosslinks are significantly more efficient than in the 162- and 172- arrays. This indicates that the H4 tails are in similar relative positions when the linker lengths corresponds to integral turns of DNA, while they are in different relative positions when the linker lengths contain an extra half turn of DNA. It is interesting to note that the H4V21C crosslink also occurs in the H2AE64C-H4V21C double mutant, and that the ratio between H4-H4 and H4-H2A crosslinks shifts depending on the NRL and state of the fibers. For example the 157 and 167 NRL fibers show more H4-H4 contacts in the compacted state than the other arrays tested, and the crosslink shifts to H4-H2A upon oligomerization. The H4-H2A crosslink is predominant in the oligomerized state for all fibers, indicating that this contact is able to out-compete the H4-H4 contact in intermolecular interactions.

The H2BA121C crosslinks form relatively efficiently across all NRLs, with disulfide bridges being more abundant in oligomeric than in the compact.

The Q44C and K113C crosslinks are weak and inefficiently formed when compared to previously described crosslinks. This might be due to the limited flexibility that these residues

have as part of helical secondary structures when compared to the flexible H4 tail and the somewhat flexible H2B C-terminus harboring A121. The H2BQ44C crosslinks can be detected in the oligomerized states, predominantly for 162 and 172 NRLs, but is absent in arrays with an NRL of 167bp. H2BK113C crosslinks are harder to detect, and are weakest for the 157-NRL arrays.

In summary, our studies show that crosslinking of specific sites on the nucleosome surface predicted by the tetranucleosome structures does occur in solution. In particular we identify the H4V21 and H2BA121 as sites of close nucleosome contacts. These two interactions are characteristic of specific tetranucleosome structures and they vary with DNA linker lengths or with the compaction state of the chromatin fiber. Therefore they have a great potential to serve as sensitive probes for monitoring chromatin fiber structure.

Discussion

Here we present two crystal structures of tetranucleosomes with an NRL of 157 bp. These structures reveal tetranucleosomes with exposed octamer faces and minimal intramolecular nucleosome-nucleosome contacts facilitated by H4 tails. The two structures are very similar, but they show differences in compactness of nucleosome packing. This shows that the 157NRL tetranucleosomes assume at least two structural states that have the potential to crystallize. This provides a lower estimate of the number of structures sampled by 157-NRL tetranucleosomes. The fact that the class averages calculated from the electron micrographs are consistent with the crystal structures argues for a relatively well defined structural population in solution that is similar to the structures observed in the crystal. A large part of the histone octamer surface is freely accessible when the tetranucleosome structures are considered in isolation, and would

permit interacting factors to directly access the chromatin fiber. In particular the acidic patch, a hot-spot for nucleosome recognition by many factors [10], is completely exposed.

The fibers observed by electron microscopy appear to be more compact and more twisted than predicted by the isolated tetranucleosome structure. The long-range regular fiber arrangement of nucleosomes is likely to impose additional structural constraints and might therefore favor an alternative mode of packing. As tetranucleosomes and 12-mer arrays were both prepared by identical crosslinking procedures it is unlikely that the glutaraldehyde crosslinking induces the compaction by itself. How the fibers exactly differ from the tetranucleosomes is unclear at the current resolution.

In the 157-NRL tetranucleosome crystals, the octamer surfaces are engaged in crystal contacts, thereby packing tetra-nucleosomes on top of each other forming columns reminiscent of the columnar phase observed in highly concentrated nucleosome preparations [42,43]. Our crystal packing provides insight into the details of how such packing can be achieved. Interestingly, we observe nucleosome interactions that use predominantly the histone H2A/H2B dimers reminiscent of the intramolecular packing observed in the 167-NRL tetranucleosome structure [11]. The interactions in the C2 form of the 157-NRL crystals strongly resemble the 167-NRL packing. In contrast, the P1 interactions are significantly shifted and they reveal a mode of interaction that has not been observed so far.

We have probed the interaction modes of nucleosomes in solution using site-specific crosslinking approaches. These experiments show clear evidence for the H4-H4 interaction and for the H2BA121 interaction, and they reveal that the NRL of fibers and the compaction or oligomerization state can modulate these nucleosome-nucleosome interactions. The Q44 and

K113 cross-links are detectable but weak, which might be due to the lower flexibility of these residues and their inability to come close enough for disulfide formation.

The structural transition of the fibers from the compacted to the oligomeric state is important to understand since this transition might be relevant for chromatin in the nuclear environment [44]. There are two options: (1) fibers compact and then keep their compacted structure while self-associating or (2) fibers are in distinct structural states when compacted and when oligomeric. Our crosslinking data provides clear evidence that new contacts are formed upon oligomerization. Whether the new contacts correspond to enhancement of contacts already present in the compact state or to contacts occurring due to structural rearrangement is difficult to say for most transitions monitored here. However, the H4-H2A crosslinking patterns in the 157-NRL, 167-NRL and 177-NRL arrays is a notable exception. The strong gain of H4-H2A cross-links at the expense of H4-H4 cross-links indicates that the structure of the arrays is indeed changing between compacted and oligomerized state. For 162-NRL and 172-NRL arrays we do not observe this shift, which indicates that the nature of the structural transition might be dependent on the NRL. The crosslinking approach is consistent with data obtained by small-angle X-ray scattering [41] for certain NRLs, but it also shows that the structural transitions might rely on a mechanism specific to the local chromatin fiber structure.

Our observations provide a framework for understanding chromatin fiber behavior in organisms with short linker DNA such as *S. pombe*. Our tetranucleosome structures are likely to be relevant for short regular stretches of genomic nucleosomes with the corresponding repeat length, which are likely to be more abundant than long arrays due to the natural chromatin fiber heterogeneity. Yeast genomes are generally very active and do not show extensive packing of nucleosomes above tetranucleosome length [19]. Our tetranucleosome structures display exposed nucleosome

surfaces ready for interaction with the nuclear machinery and predict that the short repeat lengths of *S. pombe* facilitate ready access to the genome. The crystal packing that we observe is likely to be relevant for inter-fiber interactions. However, how nucleosomes pack in the genome against their neighboring nucleosomes or against other chromatin fibers remains to be determined. Our disulfide crosslinking sites have the potential to be developed into sensitive tools to further examine higher order chromatin structures in a genomic context.

Materials and Methods

DNA and histone protein preparation

DNA molecules comprising 4x158, 4x156, 4x155, 4x154, 4x153, 4x152, 4x151, 4x150 and 4x147 NRL tandem repeats of the "601" sequence, were cloned by Gibson Assembly cloning protocol [45] and purified as described [8]. The same procedure was followed for 12x172, 12x167, 12x162, 12x157 and 4x157 which were cloned by restriction and ligation cloning. Wild type and mutant *X. laevis* histones were expressed in *E. coli* and purified as described [8] with following modifications. After resolubilization of the histone inclusion body pellet in 7M guanidium hydrochloride buffer was exchanged on a GE 26/10 desalting column with 8M urea and histones were purified on a GE Hi Trap SP/FF ion exchange column. Cysteine replacement mutations in H2B were introduced by site directed mutagenesis and purified as previously described [6]. To refold histone octamers equimolar amounts of the four histones H2A, H2B, H3 and H4 were co-folded to octamer. In all octamers containing cysteine replacement mutants the H3-C110A mutant was used and refolding was done in the presence of 20 mM β-mercaptoethanol. Intact octamers were separated from aggregated material and sub-octameric complexes using Superdex 200 (GE Healthcare) chromatography.

Nucleosome array assembly

4x- or 12x- repeat DNA and recombinant histone octamers were assembled into nucleosome arrays as described [8]. Wild type histones were replaced with cysteine replacement mutants were required. Histone octamers and DNA were mixed in the presence of 100 mM DTT, and dialysis solutions used for assembly contained 20 mM β-mercaptoethanol when cysteine replacement mutant histones were used. Assembled arrays were stored on ice. Quality of arrays was determined by ScaI restriction enzyme digestion and analysis on Native-APAGE (Agarose polyacrylamide gel electrophoresis) as shown in Fig. S1.

Tetranucleosome crystallization

Nucleosome arrays containing 4x158bp, 4x157bp, 4x156bp, 4x155bp, 4x154bp, 4x153bp, 4x152bp, 4x151bp, 4x150bp and 4x147bp were concentrated to 6 mg ml^{-1} in a solution of 10 mM KCl, 0.25 mM EDTA and 10 mM Tris-Cl, pH 7.5. Crystals were grown by vapour diffusion, mixing the tetranucleosomes with an equal volume of crystallization solution to obtain an initial concentration of 30-60 mM KCl, 90-110 mM $MgCl_2$ and 5 mM Na-cacodylate, pH 6. The drops were "salted in" against a reservoir at half the concentration of the initial condition. Crystals were transferred stepwise to 26% 2-methyl-2,4-pentanediol, 25 mM KCl, 50 mM $MgCl_2$ and 10 mM K-cacodylate, pH 6.0 before cryo-cooling in liquid nitrogen.

Structure determination

X-ray diffraction data were collected using the PXI and PXIII beamline at the Swiss Light Source (Villigen PSI, Switzerland). Integration, scaling and space group determination of diffraction data was done with XDS [46], blend and aimless [47]. Molecular replacement solutions

were found with Phaser [48] using the structure of the nucleosome core particle (PDB ID:3LZ1) [35] as search model. Rigid body and B factor refinement were done with Phenix [49]. Model building was done Coot [50]. Illustrations were prepared with PyMOL (http://www.pymol.org/).

Disulfide crosslinking

Crosslinking of 12x- nucleosome arrays was carried out as described [6,8] with slight differences. Cysteine mutations Q44C, A121C and K113C were each introduced into histone H2B by site-directed mutagenesis. Histone octamers containing cysteine mutants were purified as previously described [6]. Following reconstitution 12-mer arrays were incubated with 100 mM DTT for 2 hours on ice and precipitated by adjusting $MgCl_2$ concentration to a final 4 mM followed by centrifugation. The supernatant was discarded and pellets were resuspended in 50 mM KCl, 0.1 mM EDTA and 10 mM Tris-Cl, pH 7.5. To study chromatin arrays in different $MgCl_2$ concentrations, 11 mM and 88 mM stock solutions of $MgCl_2$ were mixed 1:10 with nucleosome arrays to yield a final concentration of 1 or 8 mM $MgCl_2$. The arrays were then mixed in a 4:1 ratio with a solution containing 250 mM Tris pH 9.0, 2.5 mM oxidized glutathione (Sigma), 2.5 mM reduced glutathione (Sigma), 50 mM KCl and 0, 1 or 8 mM $MgCl_2$ at 22 ℃. After overnight incubation , the reaction was quenched by addition of 10 mM iodoacetamide at 22 ℃ for 1 h in the dark. The samples were analyzed by non-reducing 18 % SDS-PAGE gel electrophoresis. Gels were scanned on a Li-Cor Odyssey infrared fluorescence scanner and the gel bands were quantified using ImageJ [51].

Electron Microscopy

Nucleosome arrays of 4x157 bp and 12x157 bp DNA at a concentration of 2 ug/ml were dialysed in buffer containing 10 mM Tris pH 7.5, 10 mM NaCl, 0.1 mM EDTA and 0.025 % glutaraldehyde for 30 minutes at 4 ℃and then redialysed in buffer containing 10 mM Tris pH 7.5, 10 mM NaCl, 0.1 mM EDTA. 5 µl of sample were applied to carbon coated grids. After 30 sec, samples were stained twice for 30 sec with 50 ul of 2 % uranyl acetate. Grids were examined with a Tecnai G2 electron microscope operating at 120 kV and images recorded on a FEI Eagle 4K CCD camera. 2D class averages for the 4x157bp samples were determined with Xmipp and Relion using Scipion [52–54].

Analytical Ultracentrifugation

Analytical ultracentrifugation experiments were carried out as previously described [8], and analyzed using sedfit [55]. 4-mer and 12-mer arrays were analysed in 10 mM Tris pH 7.5, 10 mM NaCl, 0.1 mM EDTA containing both 0 mM and 1 mM $MgCl_2$.

Author Contributions

Conceptualization, B.E., T.S.; Methodology, B.E., T.S.; Investigation, B.E., T.S.; Writing – Original Draft, B.E., T.S.; Writing – Review & Editing, B.E., T.J.R., T.S.; Resources, T.J.R,T.S.; Funding Acquisition, T.J.R, T.S.; Supervision, T.J.R., T.S.

Acknowledgements

We thank Yvan Pfister, Sylwia Duda, Kyoko Hashimoto and David Sargent for technical support. We acknowledge the European Synchrotron Radiation Facility (ESRF) and the Swiss Light Source at the Paul Scherrer Institut, Villigen (SLS), Switzerland for provision of

synchrotron radiation facilities and thank Vincent Olieric for assistance in using beamlines PXI and PXIII respectively. We thank Paul Guichard, Christoph Bauer and the Bioimaging Center of the University of Geneva for support with electron microscopy. We thank Alexander Adibekian and Robbie Loewith for providing access to fluorescence scanners.

Funding

B.E.: iGE3 Ph.D. salary award

T.J.R.: European Research Council Grant FP/2007-2013/Agreement 322778

T.S.: Swiss National Science Foundation SNF Professorship (PP00P3_139137, PP00P3_163760), Republic and Canton of Geneva, Fondation Ernst et Lucie Schmidheiny, Fonds Constantin Topali and Société Académique de Genève.

Accession codes

Coordinates and structure factors have been deposited in the Protein Data Bank under accession codes 5OXV and 5OY7.

Competing interests

The authors declare that they have no competing interests.

References

1. Kornberg, R.D. (1974). Chromatin structure: a repeating unit of histones and DNA. *Science* **184**, 868–871
2. Felsenfeld, G. & Groudine, M. (2003). Controlling the double helix. *Nature* **421**, 448–453
3. Luger, K., Dechassa, M.L. & Tremethick, D.J. (2012). New insights into nucleosome and chromatin structure: an ordered state or a disordered affair? *Nat. Rev. Mol. Cell Biol.* **13**, 436–447
4. Luger, K., Mäder, A.W., Richmond, R.K., Sargent, D.F. & Richmond, T.J. (1997). Crystal structure of the nucleosome core particle at 2.8 A resolution. *Nature* **389**, 251–260

5. Luger, K. & Richmond, T.J. (1998). The histone tails of the nucleosome. *Curr. Opin. Genet. Dev.* **8**, 140–146
6. Dorigo, B., Schalch, T., Kulangara, A., Duda, S., Schroeder, R.R. & Richmond, T.J. (2004). Nucleosome arrays reveal the two-start organization of the chromatin fiber. *Science* **306**, 1571–1573
7. Shogren-Knaak, M., Ishii, H., Sun, J.-M., Pazin, M.J., Davie, J.R. & Peterson, C.L. (2006). Histone H4-K16 acetylation controls chromatin structure and protein interactions. *Science* **311**, 844–847
8. Dorigo, B., Schalch, T., Bystricky, K. & Richmond, T.J. (2003). Chromatin fiber folding: requirement for the histone H4 N-terminal tail. *J. Mol. Biol.* **327**, 85–96
9. Kalashnikova, A.A., Porter-Goff, M.E., Muthurajan, U.M., Luger, K. & Hansen, J.C. (2013). The role of the nucleosome acidic patch in modulating higher order chromatin structure. *J. R. Soc. Interface* **10**, 20121022
10. McGinty, R.K. & Tan, S. (2015). Nucleosome structure and function. *Chem. Rev.* **115**, 2255–2273
11. Schalch, T., Duda, S., Sargent, D.F. & Richmond, T.J. (2005). X-ray structure of a tetranucleosome and its implications for the chromatin fibre. *Nature* **436**, 138–141
12. Song, F., Chen, P., Sun, D., Wang, M., Dong, L., Liang, D., Xu, R.-M., Zhu, P. & Li, G. (2014). Cryo-EM study of the chromatin fiber reveals a double helix twisted by tetranucleosomal units. *Science* **344**, 376–380
13. Fierz, B., Chatterjee, C., McGinty, R.K., Bar-Dagan, M., Raleigh, D.P. & Muir, T.W. (2011). Histone H2B ubiquitylation disrupts local and higher-order chromatin compaction. *Nat. Chem. Biol.* **7**, 113–119
14. Hsieh, T.-H.S., Weiner, A., Lajoie, B., Dekker, J., Friedman, N. & Rando, O.J. (2015). Mapping Nucleosome Resolution Chromosome Folding in Yeast by Micro-C. *Cell* **162**, 108–119
15. Li, W., Chen, P., Yu, J., Dong, L., Liang, D., Feng, J., Yan, J., Wang, P.-Y., Li, Q., Zhang, Z., Li, M. & Li, G. (2016). FACT Remodels the Tetranucleosomal Unit of Chromatin Fibers for Gene Transcription. *Mol. Cell* **64**, 120–133
16. Eltsov, M., Maclellan, K.M., Maeshima, K., Frangakis, A.S. & Dubochet, J. (2008). Analysis of cryo-electron microscopy images does not support the existence of 30-nm chromatin fibers in mitotic chromosomes in situ. *Proc. Natl. Acad. Sci. U. S. A.* **105**, 19732–19737
17. Nishino, Y., Eltsov, M., Joti, Y., Ito, K., Takata, H., Takahashi, Y., Hihara, S., Frangakis, A.S., Imamoto, N., Ishikawa, T. & Maeshima, K. (2012). Human mitotic chromosomes consist predominantly of irregularly folded nucleosome fibres without a 30-nm chromatin structure. *EMBO J.* **31**, 1644–1653
18. Ricci, M.A., Manzo, C., García-Parajo, M.F., Lakadamyali, M. & Cosma, M.P. (2015). Chromatin fibers are formed by heterogeneous groups of nucleosomes in vivo. *Cell* **160**, 1145–1158
19. Chen, C., Lim, H.H., Shi, J., Tamura, S., Maeshima, K., Surana, U. & Gan, L. (2016). Budding yeast chromatin is dispersed in a crowded nucleoplasm in vivo. *Mol. Biol. Cell* **27**, 3357–3368
20. Risca, V.I., Denny, S.K., Straight, A.F. & Greenleaf, W.J. (2017). Variable chromatin structure revealed by in situ spatially correlated DNA cleavage mapping. *Nature* **541**, 237–241
21. Rydberg, B., Holley, W.R., Mian, I.S. & Chatterjee, A. (1998). Chromatin conformation in living cells: support for a zig-zag model of the 30 nm chromatin fiber. *J. Mol. Biol.* **284**, 71–84
22. Woodcock, C.L., Grigoryev, S.A., Horowitz, R.A. & Whitaker, N. (1993). A chromatin folding model that incorporates linker variability generates fibers resembling the native structures. *Proc. Natl. Acad. Sci. U. S. A.* **90**, 9021–9025
23. Routh, A., Sandin, S. & Rhodes, D. (2008). Nucleosome repeat length and linker histone stoichiometry determine chromatin fiber structure. *Proc. Natl. Acad. Sci. U. S. A.* **105**, 8872–8877
24. Collepardo-Guevara, R. & Schlick, T. (2014). Chromatin fiber polymorphism triggered by variations of DNA linker lengths. *Proc. Natl. Acad. Sci. U. S. A.* **111**, 8061–8066
25. Sproul, D., Gilbert, N. & Bickmore, W.A. (2005). The role of chromatin structure in regulating the expression of clustered genes. *Nat. Rev. Genet.* **6**, 775–781
26. Gottesfeld, J.M. & Melton, D.A. (1978). The length of nucleosome-associated DNA is the same in both transcribed and nontranscribed regions of chromatin. *Nature* **273**, 317–319

27. Chereji, R.V., Kan, T.-W., Grudniewska, M.K., Romashchenko, A.V., Berezikov, E., Zhimulev, I.F., Guryev, V., Morozov, A.V. & Moshkin, Y.M. (2016). Genome-wide profiling of nucleosome sensitivity and chromatin accessibility in Drosophila melanogaster. *Nucleic Acids Res.* **44**, 1036–1051
28. Godde, J.S. & Widom, J. (1992). Chromatin structure of Schizosaccharomyces pombe. A nucleosome repeat length that is shorter than the chromatosomal DNA length. *J. Mol. Biol.* **226**, 1009–1025
29. Lantermann, A.B., Straub, T., Strålfors, A., Yuan, G.-C., Ekwall, K. & Korber, P. (2010). Schizosaccharomyces pombe genome-wide nucleosome mapping reveals positioning mechanisms distinct from those of Saccharomyces cerevisiae. *Nat. Struct. Mol. Biol.* **17**, 251–257
30. Moyle-Heyrman, G., Zaichuk, T., Xi, L., Zhang, Q., Uhlenbeck, O.C., Holmgren, R., Widom, J. & Wang, J.-P. (2013). Chemical map of Schizosaccharomyces pombe reveals species-specific features in nucleosome positioning. *Proc. Natl. Acad. Sci. U. S. A.* **110**, 20158–20163
31. Morris, N.R. (1976). Nucleosome structure in Aspergillus nidulans. *Cell* **8**, 357–363
32. Woodcock, C.L., Skoultchi, A.I. & Fan, Y. (2006). Role of linker histone in chromatin structure and function: H1 stoichiometry and nucleosome repeat length. *Chromosome Res.* **14**, 17–25
33. Thomas, J.O. & Thompson, R.J. (1977). Variation in chromatin structure in two cell types from the same tissue: a short DNA repeat length in cerebral cortex neurons. *Cell* **10**, 633–640
34. Makarov, V.L., Lejnine, S., Bedoyan, J. & Langmore, J.P. (1993). Nucleosomal organization of telomere-specific chromatin in rat. *Cell* **73**, 775–787
35. Vasudevan, D., Chua, E.Y.D. & Davey, C.A. (2010). Crystal structures of nucleosome core particles containing the "601" strong positioning sequence. *J. Mol. Biol.* **403**, 1–10
36. Makde, R.D., England, J.R., Yennawar, H.P. & Tan, S. (2010). Structure of RCC1 chromatin factor bound to the nucleosome core particle. *Nature* **467**, 562–566
37. Davey, C.A., Sargent, D.F., Luger, K., Maeder, A.W. & Richmond, T.J. (2002). Solvent mediated interactions in the structure of the nucleosome core particle at 1.9 a resolution. *J. Mol. Biol.* **319**, 1097–1113
38. Koslover, E.F., Fuller, C.J., Straight, A.F. & Spakowitz, A.J. (2010). Local geometry and elasticity in compact chromatin structure. *Biophys. J.* **99**, 3941–3950
39. de la Torre, J.G., Echenique, G. del R. & Ortega, A. (2007). Improved calculation of rotational diffusion and intrinsic viscosity of bead models for macromolecules and nanoparticles. *J. Phys. Chem. B* **111**, 955–961
40. Hansen, J.C. (2002). Conformational dynamics of the chromatin fiber in solution: determinants, mechanisms, and functions. *Annu. Rev. Biophys. Biomol. Struct.* **31**, 361–392
41. Maeshima, K., Rogge, R., Tamura, S., Joti, Y., Hikima, T., Szerlong, H., Krause, C., Herman, J., Seidel, E., DeLuca, J., Ishikawa, T. & Hansen, J.C. (2016). Nucleosomal arrays self-assemble into supramolecular globular structures lacking 30-nm fibers. *EMBO J.* **35**, 1115–1132
42. Leforestier, A., Dubochet, J. & Livolant, F. (2001). Bilayers of nucleosome core particles. *Biophys. J.* **81**, 2414–2421
43. Mangenot, S., Leforestier, A., Durand, D. & Livolant, F. (2003). Phase diagram of nucleosome core particles. *J. Mol. Biol.* **333**, 907–916
44. Maeshima, K., Imai, R., Tamura, S. & Nozaki, T. (2014). Chromatin as dynamic 10-nm fibers. *Chromosoma* **123**, 225–237
45. Gibson, D.G., Young, L., Chuang, R.-Y., Venter, J.C., Hutchison, C.A., 3rd & Smith, H.O. (2009). Enzymatic assembly of DNA molecules up to several hundred kilobases. *Nat. Methods* **6**, 343–345
46. Kabsch, W. (2010). XDS. *Acta Crystallogr. D Biol. Crystallogr.* **66**, 125–132
47. Evans, P.R. & Murshudov, G.N. (2013). How good are my data and what is the resolution? *Acta Crystallogr. D Biol. Crystallogr.* **69**, 1204–1214
48. McCoy, A.J., Grosse-Kunstleve, R.W., Adams, P.D., Winn, M.D., Storoni, L.C. & Read, R.J. (2007). Phaser crystallographic software. *J. Appl. Crystallogr.* **40**, 658–674
49. Afonine, P.V., Grosse-Kunstleve, R.W., Echols, N., Headd, J.J., Moriarty, N.W., Mustyakimov, M.,

Terwilliger, T.C., Urzhumtsev, A., Zwart, P.H. & Adams, P.D. (2012). Towards automated crystallographic structure refinement with phenix.refine. *Acta Crystallogr. D Biol. Crystallogr.* **68**, 352–367
50. Emsley, P. & Cowtan, K. (2004). Coot: model-building tools for molecular graphics. *Acta Crystallogr. D Biol. Crystallogr.* **60**, 2126–2132
51. Schindelin, J., Rueden, C.T., Hiner, M.C. & Eliceiri, K.W. (2015). The ImageJ ecosystem: An open platform for biomedical image analysis. *Mol. Reprod. Dev.* **82**, 518–529
52. Scheres, S.H.W., Núñez-Ramírez, R., Sorzano, C.O.S., Carazo, J.M. & Marabini, R. (2008). Image processing for electron microscopy single-particle analysis using XMIPP. *Nat. Protoc.* **3**, 977–990
53. Scheres, S.H.W. (2012). RELION: implementation of a Bayesian approach to cryo-EM structure determination. *J. Struct. Biol.* **180**, 519–530
54. de la Rosa-Trevín, J.M., Quintana, A., Del Cano, L., Zaldívar, A., Foche, I., Gutiérrez, J., Gómez-Blanco, J., Burguet-Castell, J., Cuenca-Alba, J., Abrishami, V., Vargas, J., Otón, J., Sharov, G., Vilas, J.L., Navas, J., Conesa, P., Kazemi, M., Marabini, R., Sorzano, C.O.S. & Carazo, J.M. (2016). Scipion: A software framework toward integration, reproducibility and validation in 3D electron microscopy. *J. Struct. Biol.* **195**, 93–99
55. Schuck, P. (2000). Size-distribution analysis of macromolecules by sedimentation velocity ultracentrifugation and lamm equation modeling. *Biophys. J.* **78**, 1606–1619

Table 1: Data Collection and Refinement Statistics

	157NRL C2	157NRL P1
Data Collection		
Space group	C121	P1
Cell dimensions:		
a, b, c (Å, °)	*348.84*, *63.27*, *271.36*	*66.6, 161.5, 227.9*
α, β, γ	*90.0, 124.7, 90.0*	78.9, 83.9, 83.7
Resolution range (Å)	223.0-6.7 (7.5-6.7) [a]	141.5-5.8 (6.2 -5.8)[a]
Wavelength (Å)	1.000	1.000
R_{merge}	0.163 (4.943)	0.110 (0.575)
Mn(I) half-set correlation CC(1/2)	0.98 (0.16)	1.00 (0.56)
Mean *I/σ(I)*	5.8 (0.3)	4.9 (1.3)
Completeness (%)	100.0 (100.0)	93.8 (83.6)
Multiplicity	6.5 (7.4)	1.9 (1.4)
Refinement		
Resolution range	71.7-6.7 (7.1-6.7)	111.4-5.8 (6.0-5.8)
Number of reflections	8045 (457)	24322 (2115)
Number of reflections in test set	1016 (63)	1226 (111)
R factor (%)	31.70 (50.85)	21.8 (36.4)
R_{free} (%)	35.22 (48.15)	23.9 (39.7)
No. of atoms - total	24647	49323
Macromolecule	24647	49315
R.m.s.d., bonds (Å)	0.009	0.011
R.m.s.d., angles (°)	1.472	1.487
Clash score	6.72	12.35
Average B factor ($Å^2$)	505	230

[a] Values in parentheses are for highest-resolution shell.

Figure legends

Figure 1: Tetranucleosomes with different nucleosome repeat lengths crystallize in different forms. (a) Crystals obtained from tetranucleomes reconstituted with wild type Xenopus histones and the indicated nucleosome repeat lengths (NRL) DNA templates. (b) Tetranucleosomes with NRL between 147 and 158 crystallize with variable diffraction limits. Space group and unit cell parameters were determined where possible and they show that tetranucleosomes can crystallize in a diverse set of crystal forms.

Figure S1: Reconstitution of tetranucleosome arrays (a) Illustration of consequences for realtive rotation between nucleosomes upon addition of linker base pairs. (b) SDS-PAGE denaturing gel of Xenopus leavis histone octamer used for reconstitution. (c) Cartoon representation of the strategy for reconstituting tetranucleosomes. (d) Native APAGE gel of reconstituted tetranucleosomes. ScaI partially digested samples show mono-, di-, tri-, tetra-nucleosomal species

Figure 2: 157NRL tetranucleosome crystal structures show exposed histone octamer surface and linker DNA. (a) 157NRL tetranucleome structure observed in crystal form P1 shown in cartoon representation (H3: blue, H4: green, H2A: red, H2B: yellow) (b) 157NRL tetranucleosome structure observed in crystal form C2. (c) Schematic representation of DNA path in 157NRL tetranucleosomes. (d) The 167NRL structure (PDB ID: 1ZBB) is shown for comparison. (e) Negative stain micrograph of 157NRL tetranucleosomes and corresponding class averages show structures similar to crystal structures in (a).

Figure S2: Electron density for 157NRL crystal forms C2 (a) and P1 (b) after molecular replacement using 601 mononucleosomes as search model and rigid body and B-factor

refinement shows clear positive density for linker DNAs. 2Fo-Fc (blue) and Fo-Fc (red/green) difference maps at 0.42 sigma after molecular replacement and rigid body and atomic displacement refinement.

Figure 3: 157NRL fibers. (a) 157NRL fiber model based on geometrical parameters determined from the crystal structures illustrates the predicted flat ribbon architecture with the central four nucleosomes superimposed onto the 157NRL P1 tetranucleosome structure. (b) Negative stain electron micrograph of 157NRL 12-mer arrays. Scale bar equals 100 nm. (c) Relion 2D major class average (44 particles) from well defined particles. Arrowheads indicate inferred nucleosome positions that are spaced at ~66 Å intervals.

Figure S3: Geometrical analysis of 157NRL tetranucleosomes reveals variability with respect to fiber axis. (a), (b) Superposition of coordinate systems onto individual nucleosomes and definition of chromatin fiber axis (black line). x axes are green, y axes blue and z axes red. (c), (d) Geometrical parameters corresponding to tetranuclesome show above table. (e) Sedfit calculation of S value distribution c(s) for 157NRL tetranucleosomes with 1 mM Mg (blue) and no Mg (orange). (f) Same c(s) analysis as in (e) for 12mer 157NRL arrays.

Figure 4: Nucleosomes use various interfaces to interact. (a) Stacking of 157NRL tetranucleomes observed in P1 crystal form with three tetranucleosomes in teal, cyan and white (histone colors, H3: blue, H4: green, H2A: red, H2B: yellow) (b) Cut through top and bottom layers of nucleosome core stacks shown in (a). (c) Close-up of the nucleosome interfaces observed in the P1 crystal packing. (d) Tetranucleosome stacking for the C2 crystal form and (e) corresponding cut through bottom nucleosome stack. (f) Close-up of nucleosome interfaces in the C2 crystal form.

Figure 5: Nucleosomes use various interfaces to interact. (a) Heatmap for distances between identical H2B residues on opposing nucleosome faces. The Cβ atoms distances are plotted for the nucleosome-nucleosome contacts observed in the different crystal structures. (b) Illustration of expected crosslinking product between two nucleosomes. (c) Nucleosome core particle in cartoon representation showing the residues chosen for crosslinking in sphere representation. (H3: blue, H4: green, H2A: red, H2B: yellow) (d) Indicated cysteine mutant histone octamers were reconstituted onto 12-mer 601 array DNA with various NRLs and crosslinked using GSH/GSSG oxidation under increasing magnesium concentrations (0, 1, 8 mM) and then run on non-reducing SDS PAGE and stained with coomassie brilliant blue. Shown are only bands resulting from crosslink products. Quantification and complete gels are shown in Fig. S5.

Figure S4: (a) Quantification and full size images related to Fig. 5d. Plotted are fractions of crosslinked signal compared to total octamer signal determined from coomassie fluorescence in ImageJ. Insets show representative examples of corresponding crosslinking experiments. Standard errors shown are derived from triplicate experiments.

(a)

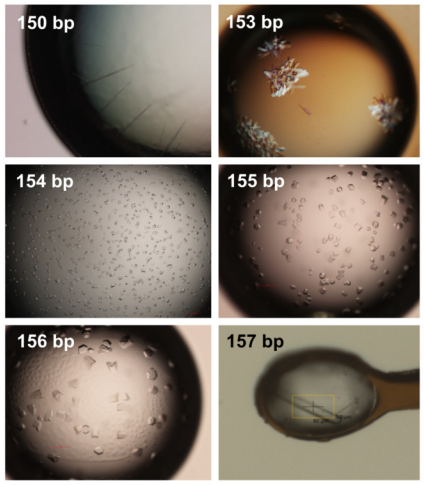

(b)

NRL	Crystals	Diffraction limit	Space group	Unit cell	Nucs/AU
147 bp	none	-	-	-	-
150 bp	single crystals	~7 Å	-	-	-
151 bp	none	-	-	-	-
152 bp	microcrystals	-	-	-	-
153 bp	crystal clusters	~20 Å	-	-	-
154 bp	single crystals	-	-	-	-
155 bp	single crystals	~25 Å	hexagonal	a=301, b=301, c=773 α=90, β=90, γ=120	4-8
156 bp	single crystals	~25 Å	hexagonal	a=300, b=300, c=382 α=90, β=90, γ=120	8-16
157 bp	single crystals	6.7 Å	C2	a=349, b=63, c=280 α=90, β=124.7, γ=90	2
157 bp	single crystals	5.8 Å	P1	a=67, b=163, c=230 α=79, β=84, γ=84	4
158 bp	single crystals	~22 Å	-	-	-

Figure 1: Tetranucleosomes with different nucleosome repeat lengths crystallize in different forms. (a) Crystals obtained from tetranucleomes reconstituted with wild type Xenopus histones and the indicated nucleosome repeat lengths (NRL) DNA templates. (b) Tetranucleosomes with NRL between 147 and 158 crystallize with variable diffraction limits. Space group and unit cell parameters were determined where possible and they show that tetranucleosomes can crystallize in a diverse set of crystal forms.

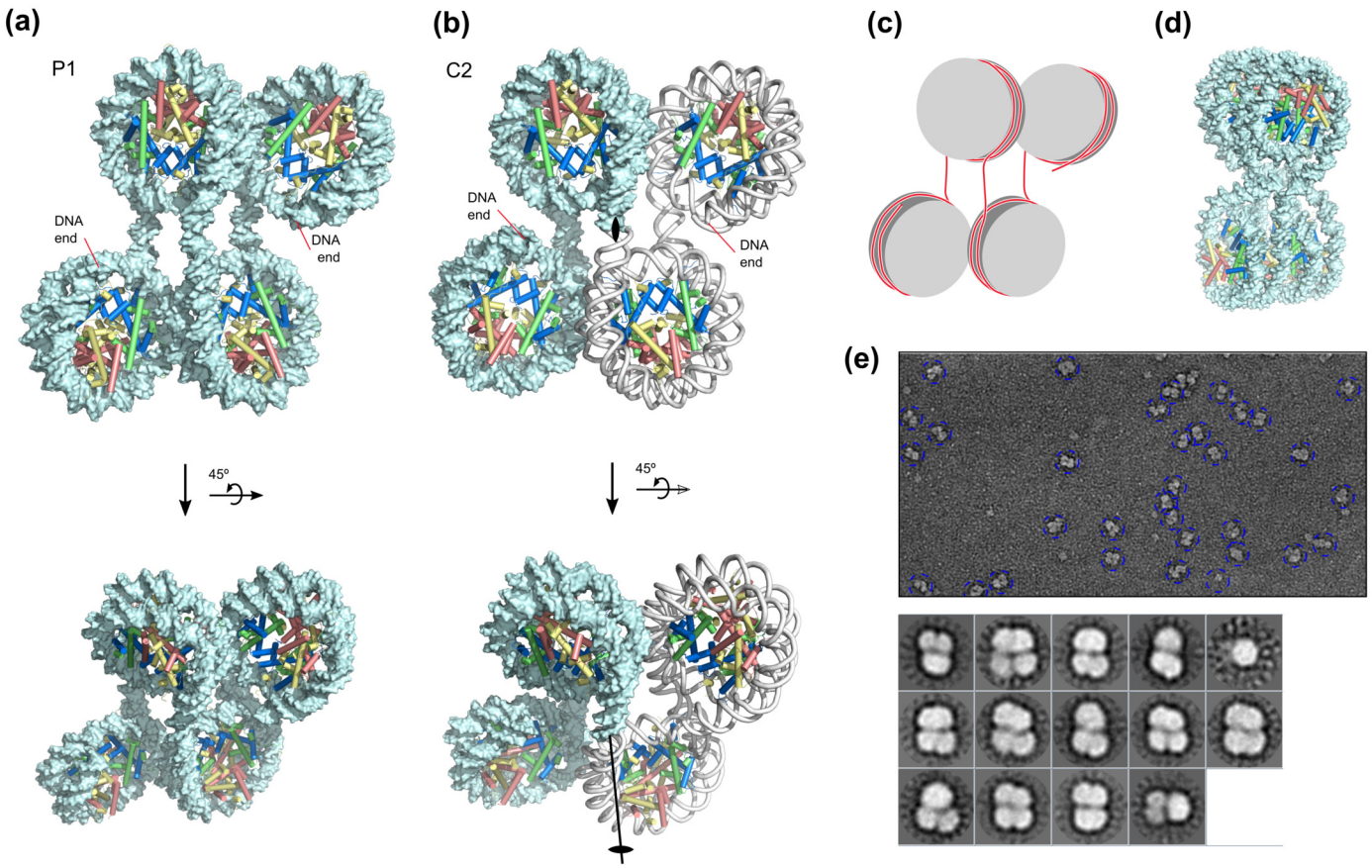

Figure 2: 157NRL tetranucleosome crystal structures show exposed histone octamer surface and linker DNA. (a) 157NRL tetranucleome structure observed in crystal form P1 shown in cartoon representation (H3: blue, H4: green, H2A: red, H2B: yellow) (b) 157NRL tetranucleosome structure observed in crystal form C2. (c) Schematic representation of DNA path in 157NRL tetranucleosomes. (d) The 167NRL structure (PDB ID: 1ZBB) is shown for comparison. (e) Negative stain micrograph of 157NRL tetranucleosomes and corresponding class averages show structures similar to crystal structures in (a).

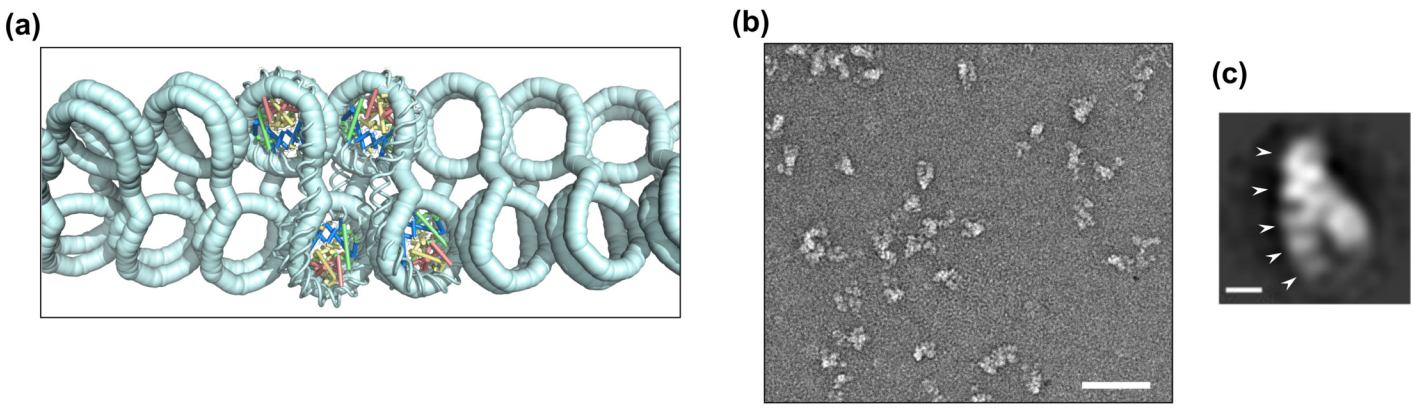

Figure 3: 157NRL fibers. (a) 157NRL fiber model based on geometrical parameters determined from the crystal structures illustrates the predicted flat ribbon architecture with the central four nucleosomes superimposed onto the 157NRL P1 tetranucleosome structure. (b) Negative stain electron micrograph of 157NRL 12-mer arrays. Scale bar equals 100 nm. (c) Relion 2D major class average (44 particles) from well defined particles. Arrowheads indicate inferred nucleosome positions that are spaced at ~66 Å intervals.

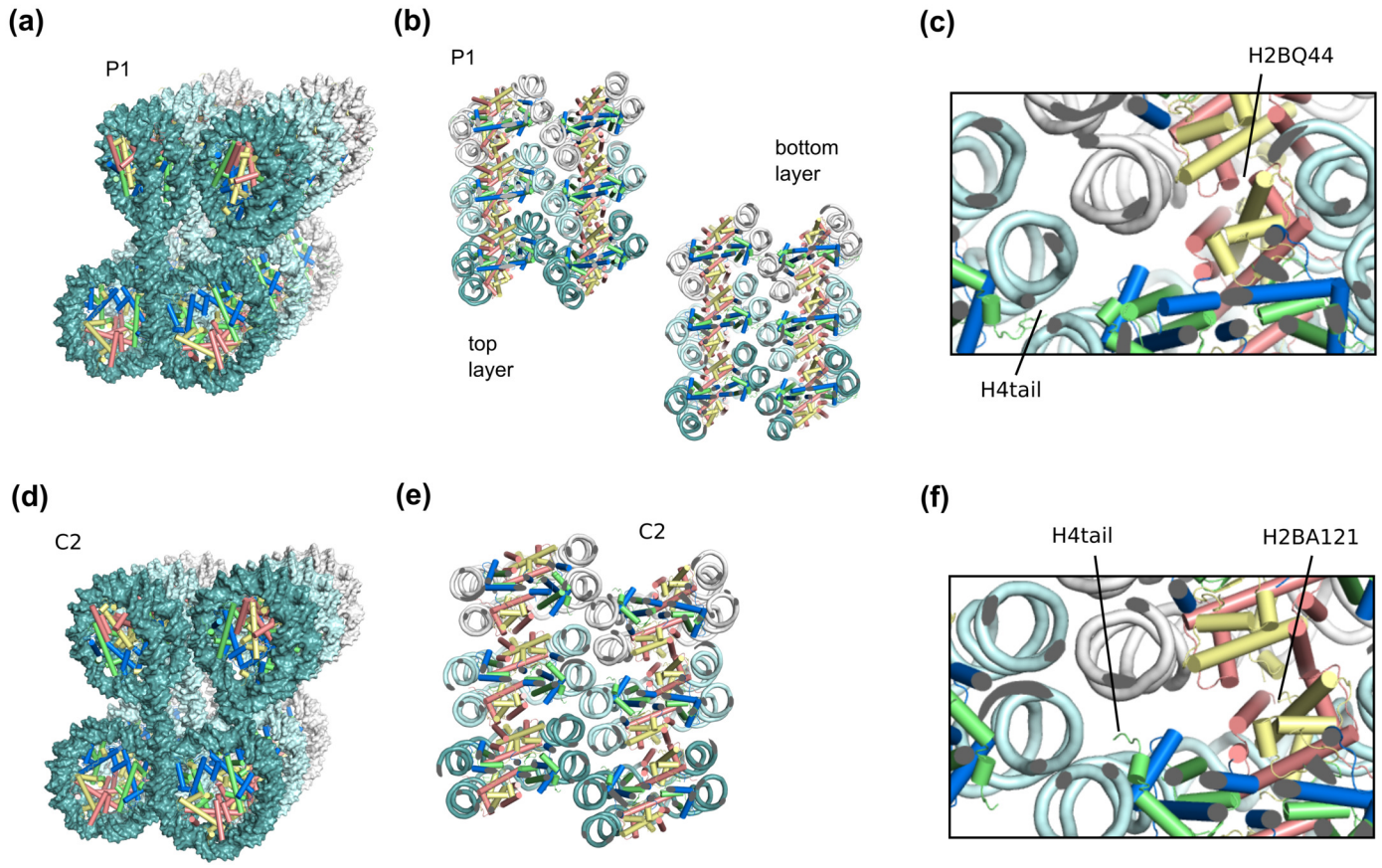

Figure 4: Nucleosomes use various interfaces to interact. (a) Stacking of 157NRL tetranucleomes observed in P1 crystal form with three tetranucleosomes in teal, cyan and white (histone colors, H3: blue, H4: green, H2A: red, H2B: yellow) (b) Cut through top and bottom layers of nucleosome core stacks shown in (a). (c) Close-up of the nucleosome interfaces observed in the P1 crystal packing. (d) Tetranucleosome stacking for the C2 crystal form and (e) corresponding cut through bottom nucleosome stack. (f) Close-up of nucleosome interfaces in the C2 crystal form.

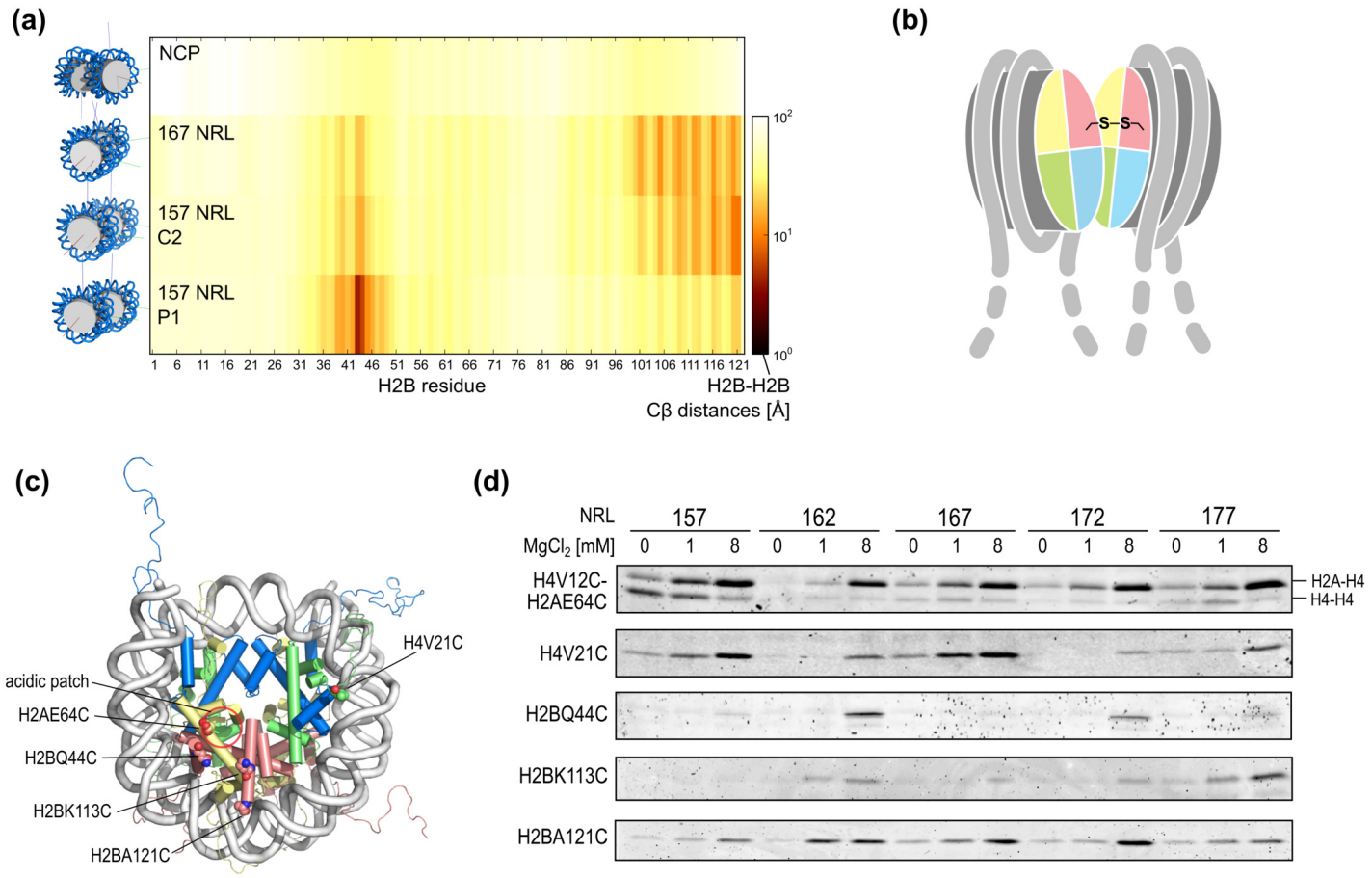

Figure 5: Nucleosomes use various interfaces to interact. (a) Heatmap for distances between identical H2B residues on opposing nucleosome faces. The Cβ atoms distances are plotted for the nucleosome-nucleosome contacts observed in the different crystal structures. (b) Illustration of expected crosslinking product between two nucleosomes. (c) Nucleosome core particle in cartoon representation showing the residues chosen for crosslinking in sphere representation. (H3: blue, H4: green, H2A: red, H2B: yellow) (d) Indicated cysteine mutant histone octamers were reconstituted onto 12-mer 601 array DNA with various NRLs and crosslinked using GSH/GSSG oxidation under increasing magnesium concentrations (0, 1, 8 mM) and then run on non-reducing SDS PAGE and stained with coomassie brilliant blue. Shown are only bands resulting from crosslink products. Quantification and complete gels are shown in Fig. S5.